ARTICLE NO. 78-1250R

Interferometric Attitude Determination with the Global Positioning System

J.F. Ellis* and G.A. Creswell†
Lockheed Missiles and Space Co. Inc., Sunnyvale, Calif.

This paper develops a linear error model for an interferometer attitude system. Using the Global Positioning System (GPS) as its signal source, this error model estimates three-axis spacecraft attitude, gyro misalignments, and gyro drift. A functional block error analysis of the interferometer receiver group is presented along with the results of a digital simulation.

Nomenclature

B_K^B = interferometer bore sight
$\bar{b}_i$ = angular alignment error
$[C_s]$ = direction cosine matrix
$[I]$ = identity matrix
L_k^B = vector between interferometer antenna pair
P^I = user spacecraft position
R_j^I = GPS satellite position
S_j^B = body frame spacecraft to jth GPS line-of-sight vector
SV_j^I = inertial spacecraft to jth GPS line-of-sight vector
γ_{jk} = interferometer electrical phase difference
Δ = small angle transformation matrix
$\Delta\theta_i$ = single-axis small-angle error
ϕ_{jk} = spatial angle between the kth interferometer and the jth GPS satellite
$\bar{\epsilon}_i$ = gyro scale factor
$\bar{\omega}_i^B$ = gyro rate bias error
$\bar{\omega}_v^B$ = true vehicle rate

Superscripts and Subscripts

B = body reference frame
I = inertial reference frame
i = coordinate axis, $i=1,2,3$
j = GPS number, $j=1,2,\ldots,24$
k = interferometer number, $k=1,2,3$
s = gyro sensed

Attitude Determination

THE basic interferometer measurement is an electrical phase difference between radio signals arriving at separate antennas. The angular orientation of the receiver antennas with respect to wave front is obtained from this phase measurement. The voltage phase difference induced at antennas 1 and 2 by a wave front arriving at an angle ϕ (see Fig. 1) is given by

$$\gamma_{jk} = (2\pi/\lambda) L_k \cdot S_j^B = (2\pi/\lambda)\,|L_k|\cos(\phi_{jk}) \qquad (1)$$

where λ is the GPS operating wavelength ($\cong 0.19$ m), L is the antenna position difference vector, and S^B is the line-of-sight vector to the GPS transmitter in the spacecraft reference frame. As shown in Refs. 1 and 2, unique determination of three-axis attitude requires that two linearly independent vectors be measured with two or more linearly independent interferometers and that the same vectors in some fixed coordinate frame be known.

This gives nine equations and six independent unknowns. The elements of the direction cosine matrix $C_{I/B}$ are then given by

$$[C]_{I/B} = \begin{bmatrix} SV_1 & SV_2 & SV_1 \times SV_2 \end{bmatrix}_I \begin{bmatrix} S_1 & S_2 & S_1 \times S_2 \end{bmatrix}_B^{-1} \qquad (2)$$

where

$$S_j^B = [\cos\phi_{j1}, \cos\phi_{j2}, \sqrt{1-\cos\phi_{j1}^2 - \cos\phi_{j2}^2}\,]^T \qquad (3)$$

and

$$SV_j^I = R_j^I - P^I \qquad (4)$$

for $j=1,2$ and $k=1,2$.

Figure 2 depicts the measurements geometry for the jth GPS satellite with interferometer bases $k=1$ and 2. In this diagram the interferometers are conincident with the spacecraft (S/C) body axis.

This formulation of the attitude problem works well with GPS because of the vectors R^I and P^I are readily available to GPS users through the basic inertial navigation function of the GPS system. However, mechanization of this algorithm does require that the operational configuration provide interferometers with overlapping fields of view and a receiver

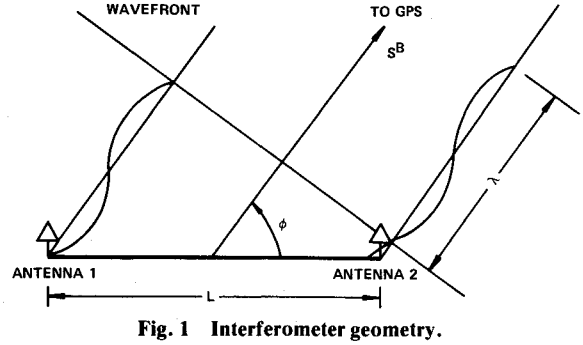

Fig. 1 Interferometer geometry.

Presented as Paper 78-1250 at the AIAA Guidance and Control Conference, Palo Alto, Calif., Aug. 7-9, 1978; submitted Sept. 5, 1978; revision received April 16, 1979.

Index categories: Guidance and Control; Sensor Systems; Spacecraft Navigation, Guidance and Flight Path Control.

*Research Engineer; presently, Sperry Flight Systems, Phoenix, Ariz. Member AIAA.
†Group Engineer.

capable of processing at least two GPS signals nearly coincident in time.

Linear Error Model

To simplify antenna and receiver requirements, a linear model was developed that would allow sequential processing of single interferometer phase measurements. In this model, the inteferometer was configured as a body fixed attitude sensor capable of providing attitude and gyro parameter error information at discrete update intervals.

Expressing the error between the true attitude $[C]$ and the gyro-sensed attitude $[C_s]$ as a small-angle transformation gives

$$[C]_{B/I} = [\Delta]\,[C_s]_{B/I} \tag{5}$$

where

$$\Delta = [I - \Delta\theta\times] = \begin{bmatrix} 1 & \Delta\theta_3 & -\Delta\theta_2 \\ -\Delta\theta_3 & 1 & \Delta\theta_1 \\ \Delta\theta_2 & -\Delta\theta_1 & 1 \end{bmatrix} \tag{6}$$

This allows $\Delta\theta_i$ to be expressed as a linear combination of alignment and gyro error parameters.[3,4] $\Delta\theta$ is then written as

$$\overline{\Delta\theta} - \bar{b} + [\bar{\omega} + \bar{\omega}_v^B \bar{\epsilon}]\,t \tag{7}$$

where $\bar{b}$ is the angular alignment error at $t=0$, $\bar{\omega}$ is the gyro rate bias errors, $\bar{\epsilon}$ is the gyro scale factor errors, and ω_v^B is the true vehicle rate.

Using the phase angle γ_{jk} from Eq. (1) and the vector S_j^B transformed from SV^I with Eq. (5),

$$S_j^B = [\Delta]\,[C_s]_{B/I}\,[SV_j^I] \tag{8}$$

gives

$$\gamma_{jk} = (2\pi/\lambda) L_k^B \cdot [\,[\Delta]\,[C_s]_{B/I}\,[SV_j^I]\,] \tag{9}$$

The phase angle observation γ with random errors v is

$$\bar{\gamma} = z = Hx + V \tag{10}$$

where the sensitivity matrix H and the state vector x are as follows:

$$H = \frac{\partial\gamma}{\partial x} \quad \text{and} \quad x = \begin{bmatrix} \bar{b} \\ \bar{\omega} \\ \bar{\epsilon} \end{bmatrix}$$

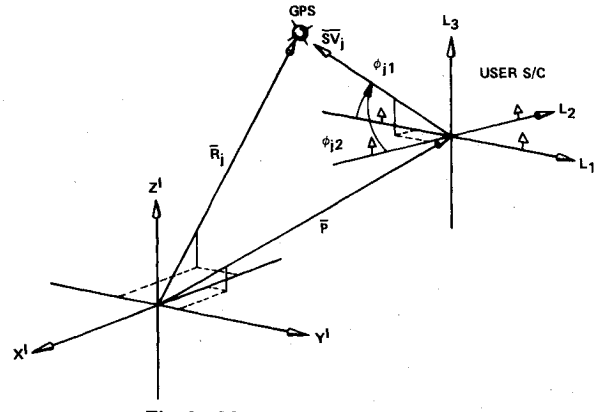

Fig. 2 Measurement geometry.

The recursive least-squares estimate of the n component state vector x is given by[5]

$$\hat{X}_{n+1} = \hat{x}_n + PH^T R^{-1}(z - Hx) \tag{11}$$

with the estimate covariance inverse

$$P^{-1} = M^{-1} + H^T R^{-1} H \tag{12}$$

and measurement noise

$$R = E(vv^T) \tag{13}$$

This mathematical construction for multiple interferometer systems allows the observations γ to be processed either sequentially or in groups, depending on the required signal dwell time and the processor/receivers capabilities. This construction has the definite advantage that the interferometers fields of view do not have to overlap and the measurements do not have to be coincident in time for the estimate to be formed.

Candidate Configuration

General Requirements

As described in the attitude measurement discussion, the minimum requirements for an operational configuration were two linearly independent interferometers and one GPS receiver capable of sequentially processing GPS signals from each of the interferometer antenna pairs. This minimum configuration, with variations in the number of interferometers and degrees of calibration, formed the basis for analysis of the attitude determination system. The basic geometry for attitude determination is similar in nature to the navigation problem,[6] and the accuracy of such a system can be improved by proper selection of GPS satellites used to form the solution. No attempt was made in this analysis to optimize the selection process.

Antenna Geometry

For the purposes of this study, antenna geometric and structural analysis was limited to the identification of interferometer fields of view and evaluation of a simple structural model for the antenna supports. The supports were characterized as cantilevered graphite epoxy beams with

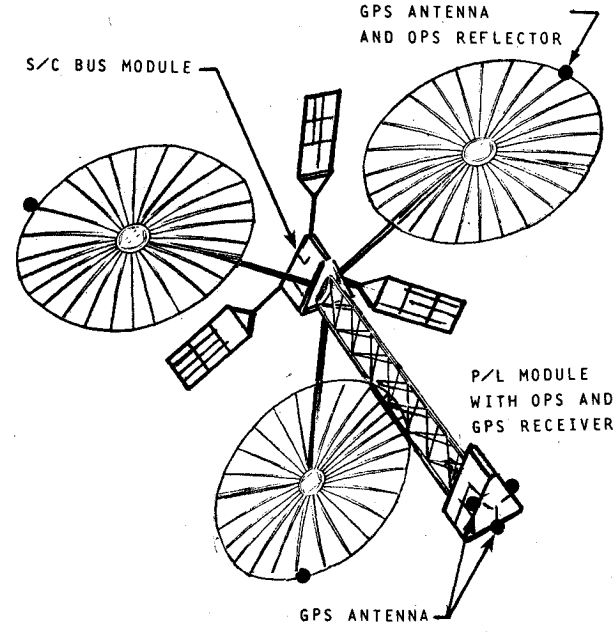

Fig. 3 Candidate interferometer application.

passive thermal control. This model should represent the types of errors incurred and give some insight as to their magnitudes with respect to the system as a whole. The interferometers' fields of view were defined by the bore sight vectors B_j where

$$\begin{bmatrix} B_1 & B_2 & B_3 \\ | & | & | \end{bmatrix} = [\psi]_3[\theta]_2[\phi]_1 \begin{bmatrix} 1 & 0 & 0 \\ 0 & 1 & 0 \\ 0 & 0 & 1 \end{bmatrix} \quad (14)$$

with Euler angles $\phi = -30$ deg, $\theta = 45$ deg, and $\psi = 0$ deg.

The minimum configuration included vectors B_1 and B_2 with the field-of-view cones defined as ± 30 deg. Figures 3 and 4 show possible antenna locations and their resulting fields of view for a geosynchronous type spacecraft. While the details of this type of structure were not included in the present analysis, the diagram does represent the concept for deployment for an interferometric attitude system.

Receiver Group

The interferometer receiver group shown in Fig. 5 meets the basic requirements for differential phase measurement for attitude determination. The system uses a standard GPS receiver and processes GPS signals at radio frequency (RF) before entering the GPS receiver to avoid the effects of nonlinearities in the GPS user receiver.

The interferometers' phase shifters are initially adjusted to an arbitrary phase angle. This high-gain mode produces useful signal levels to the receiver for initial acquisition. After the tracking loop is locked, the direction finding or phase angle determination is made by adjusting the phase shifters until a null is detected in the selected GPS channel. The phase of the RF output is then just the supplement of the total phase angle induced by the computer-controlled phase shifters. If long signal integration times are required due to low signal levels, it may be necessary to resynchronize the channel clock. This re-synchronization can be accomplished by either comparing the clock with other receiver channels or by returning to the high-gain mode for short periods of time. The return rate and return time to clock synchronization would be determined by the received signal levels and clock drift rate.

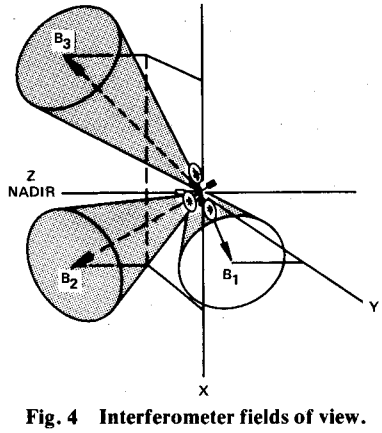

Fig. 4 Interferometer fields of view.

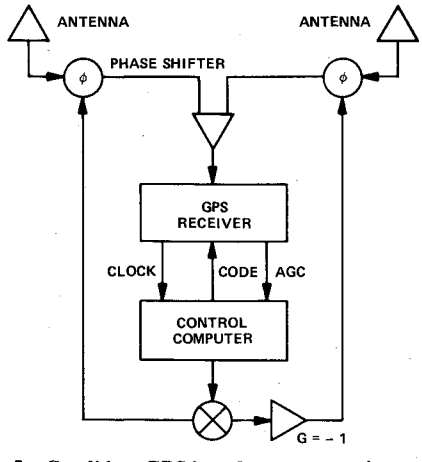

Fig. 5 Candidate GPS interferometer receiver group.

Errors and Calibration

Because the errors induced by the GPS system are small compared to other sources, the interferometric attitude determination accuracy depends on the ability to calibrate and compensate interferometer system and environmental errors. This calibration can be accomplished at several levels of precision during flight or preflight phases.

1) *Prelaunch calibration* would include an active interferometer measurement of a known attitude and the use of compensating cable loops during flight to compensate for changes induced by uneven heating and flexing of antenna cables.

2) *Postlaunch calibration* would require a known attitude measurement after launch and final deployment of the interferometer antenna system. This scheme might also include modeling of the systems deterministic error sources.

3) *Continuous calibration* would use active onboard measurements to calibrate and compensate the interferometer. This could include a radio frequency reflectometer and an optical position sensor. The reflectometer would measure cable length changes due to heating and flexing and the optical sensor would measure the deflections to compensate for structural misalignments and flexure. Structural flexure is a major error source in limber, long baseline interferometers.

Table 1 summarizes the component errors for several types of calibrations. The expected electrical phase measurement errors range from 58 to 4 deg for the 100λ system and 8.3 to 2.7 deg for the 10λ system. These phase errors result in 1σ single-axis attitude errors of 0.09-0.006 deg and 0.13-0.043 deg, respectively.

The component errors in Table 1 were evaluated at a constant signal integration time (100 s) and a constant thermal gradient across antenna supports (70°F/in.). System sensitivity to these two parameters is illustrated in Figs. 6 and 7. The response of the long baseline interferometer to thermal variations indicates the need for some type of active measurement to compensate for structural flexure. The geometry of the interferometer also results in a sensitivity to the observation angle. This effect is inversely proportional to the sine of the observation angle. Figure 8 shows the error contribution for four configurations. Constraining the interferometers field of view to ± 30 deg limits this effect.

Performance Analysis

GDOP and Convergence

The Geometric Dilution of Precision (GDOP) is a performance index which indicates to what degree the geometry of the problem magnifies or smears the measurement error v into the estimate of the state x. It is defined by the diagonal terms of the covariance matrix:

$$P = [H^T R^{-1} H^T]^{-1} \quad (15)$$

with $[R]$ the noise matrix set equal to unity.

As shown in Ref. 6, the GDOP for the navigation problem is a function of the relative position of the user and the GPS satellites being tracked. An inspection of Eq. (9) indicates a more complex situation for the attitude problem.

Table 1 Estimated component errors 100λ baseline interferometer

Receiver group	Basic system	Prelaunch calibration with compensating cable loops	Postlaunch calibration	Continuous calibration: RF reflectometer and optical position sensor
Cables				
Manufacturing tolerances	2.0	1.0	0.2	0.2
Uneven heating	31.5	3.15	3.15	3.15
Flexing	8.2	20.1	2.10	0.8
Phase shifters				
Manufacturing tolerances	3.0	1.0	1.0	1.0
Random errors	3.6	1.0	1.0	1.0
VSWR	2.8	2.8	2.8	1.4
Power combiner				
Manufacturing tolerances	3.0	1.0	1.0	1.0
Random	0.1	0.1	0.1	0.1
Receiver				
Null uncertainty	0.26	0.26	0.26	0.26
RSS Subtotal	33.2	20.6	5.1	3.9
Mounting and structural contributions				
Antenna				
Orientation	0.1	0.1	0.1	0.1
Rotation	2.5	2.5	2.5	0.25
Deflection	48.0	48.0	48.0	0.5
RSS Subtotal	48.1	48.1	48.1	0.56
RSS Total	58.4	52.3	48.3	4.0
Estimated component errors 10λ baseline interferometer				
RSS Total, deg	8.35	10.83	2.77	2.77

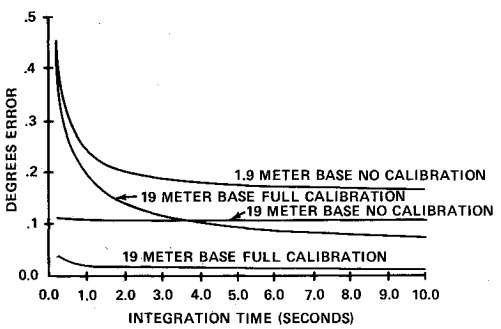

Fig. 6 Single-axis attitude error vs signal integration time.

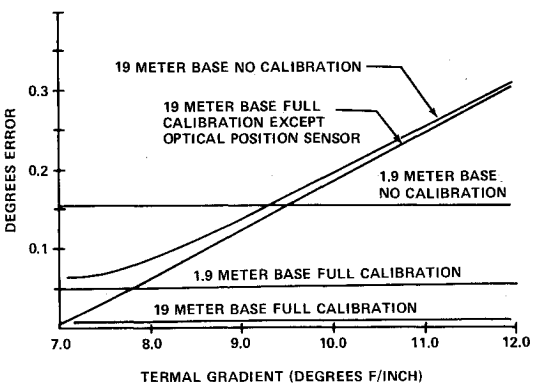

Fig. 7 Single-axis attitude error vs thermal gradient.

Following Ref. 3 for an examination of the least-squares convergence characteristics, the estimate of a constant C in the presence of noise v_i is given by

$$\hat{C} = \frac{1}{N}\sum_{i=1}^{N}(C+v_i) = C + \frac{1}{N}\sum_{i=1}^{N} v_i \tag{16}$$

which results in

$$\sigma_c^2 = \sigma_v^2/N \tag{17}$$

where σ_v^2 is the variance in the measurement noise; v_i and N are the number of measurements.

Assuming a single-axis rotation and rewriting Eq. (9) using the average values of S^B, $\bar{t}$, and $\bar{\omega}_v$, gives the average value of the phase measurement γ between updates as

$$\bar{\gamma} = (2\pi/\lambda)\,[L_1\bar{s}_2(\bar{b}_3 + \omega_3\bar{t} + \omega_v\epsilon_3\bar{t}) + L_1\bar{s}_1] \tag{18}$$

where $\bar{s}$ is the average unit vector of S^B. For simplicity, $\bar{L}$ was chosen along the body axis L_1 (see Fig. 2). Treating the terms in Eq. (18) separately and setting them equal to σ_c^2 the variances of the gyro error parameters are

$$\sigma_b^2 = \left[\frac{\sigma_v\lambda}{2\pi\sqrt{N}L_1\bar{s}_2}\right]^2 \tag{19}$$

$$\sigma_\omega^2 = \left[\frac{\sigma_v\lambda}{2\pi\sqrt{N}L_1\bar{t}\bar{s}_2}\right]^2 \tag{20}$$

$$\sigma_\epsilon = \left[\frac{\sigma_v\lambda}{2\pi\sqrt{N}L_1\bar{s}_2\bar{t}\omega_v}\right]^2 \tag{21}$$

These results indicate that we can expect at least a $1/\sqrt{N}$ convergence for all three gyro error parameters as a function of the sample number N.

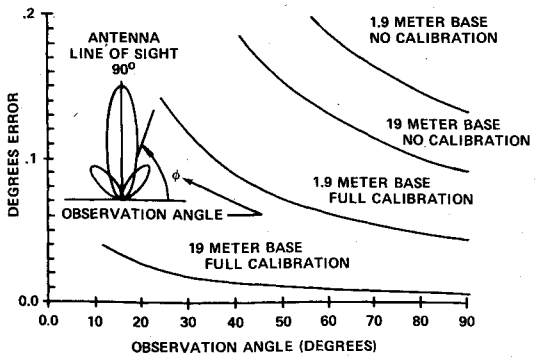

Fig. 8 Single-axis attitude error vs observation angle.

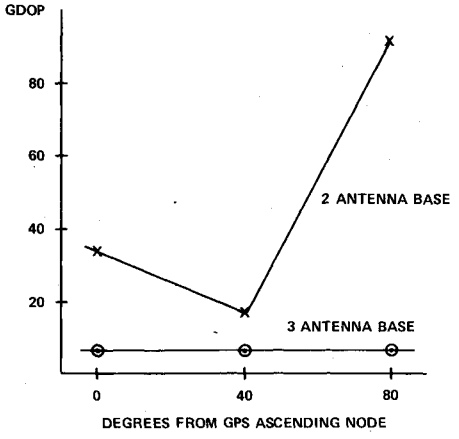

Fig. 9 Misalignment GDOP vs ascending node location.

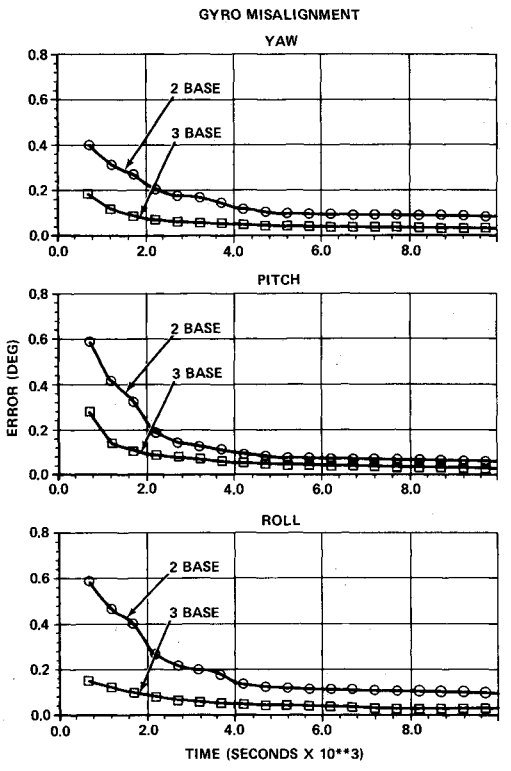

Fig. 10 One sigma time histories (400 n.mi. orbit).

If the diagonal terms of R (i.e., σ_v^2) are set equal to unity, Eqs. (19-21) also give an estimate of the GDOP characteristics for each element in the state after N measurements. It is interesting to point out that since $\bar{s}_2$ is the average unit vector component along the bore sight of the interferometers' field of view, it is equal to $\sin(\bar{\phi})$, where $\bar{\phi}$ is the average observation angle. The $1/\sin(\phi)$ sensitivity was previously shown in Fig. 8.

Digital Simulation

The performance characteristics of the GPS interferometer systems were investigated by mechanizing the linear error model in a six-degree-of-freedom digital simulation. The configuration studies assumed the user spacecraft was nadir pointing with no external disturbances and that the GPS network was fully operational with 24 satellites. Receiver group and structural errors were included in the attitude determination and parameter estimation evaluation. Because $d\omega_v/dt = 0$, the scale factor parameter was not observable in the cases examined. However, Coffman has already shown for ω_y not constant that the scale factor is observable for cases similar in nature to the one examined herein.[3,4]

Figure 9 shows the relative sensitivity of the misalignment parameter to user orbit ascending node position relative to the GPS network for two- and three-field-of-view interferometer systems.

For the two-field-of-view case, the interferometer corresponding to the boresight vector B_3 was not used. The

Table 2 Gyro parameter accuracy summary

2 FOV[a] / 3 FOV		400 n.mi. orbit I	II	III	IV	Geosynchronous orbit[b] I	II	III	IV[c]
10-m base (10λ)	σ_b(deg)	.50 / .30	.63 / .39	.17 / .11	.17 / .11	.45	.59	.16	.16
	$\sigma_\omega\left(\frac{\text{deg}}{10^3\text{s}}\right)$	.044 / .029	.055 / .037	.015 / .010	.015 / .010	.006	.008	.002	.002
19-m base (100λ)	σ_b(deg)	.35 / .22	.31 / .19	.30 / .18	.03 / .02	.34	.29	.27	.02
	$\sigma_\omega\left(\frac{\text{deg}}{10^3\text{s}}\right)$	.031 / .022	.027 / .018	.002 / .010	.002 / .001	.005	.004	.003	.001

[a] FOV = field of view.
[b] 2 FOV case not examined.
[c] I = no calibration, II = preflight calibration, III = post deployment calibration (one time), IV = continuous onboard calibration.

reference orbit for this case was 400 n.mi. circular with an inclination of 107 deg. The GDOP in these two figures is the position contribution only (i.e., $\lambda/2\pi L$ was set equal to unity) and is representative of approximately 30 samples at 100-s intervals with 2-3 measurements (γ) per sample. The three-field-of-view system displayed an approximate value of 6 over the range examined, while the two-field-of-view system varied considerably.

Gyro misalignment parameter 1σ time histories for a fully calibrated 100λ baseline interferometer are shown in Fig. 10 for a 400 n.mi. circular orbit. Misalignment accuracies of approximately 0.04 deg (3 FOV) and 0.8 deg (2 FOV) are achieved after 1 revolution (6000 s). Rate bias accuracies were better than 0.002 deg per 1000 s for both 3 and 2 FOV systems. Similar results were also obtained for a 3 FOV geosynchronous orbit configuration. In all cases examined, both misalignment and rate bias parameters displayed the predicted $1/\sqrt{N}$ type convergence. The leveling effect noticed in the two baseline interferometer data is attributed to samples with one or no measurements.

Table 2 summarizes the parameter estimation performance for several configurations in medium and geosynchronous orbit geometries. Misalignment accuracies ranged from 0.63 deg 1σ to 0.02 deg 1σ after two revolutions of data, while rate bias parameter estimation was from 0.05 deg/1000 s to less than 0.001 deg/1000 s.

Summary and Conclusions

The linear error model developed allowed simplification of the necessary hardware for interferometric attitude determination. Nonoverlapping fields of view reduced the number of antennas required, and sequential processing of the GPS signals required only a single-channel GPS receiver. A functional error analysis of the resulting interferometer attitude determination system identified the need for prelaunch or postlaunch calibrations for a 1.9 m baseline interferometer and continuous onboard calibrations for 19-m baseline systems. Radio frequency reflectometry and optical position measurements were implemented in the onboard calibration scheme. The results of a six-degree-of-freedom digital simulation pointed out the sensitivity of a 2 FOV interferometer to orbital geometry. The evaluation of gyro parameter estimation indicated a stable performance for medium and geosynchronous orbits with two- and three-field-of-view interferometers. Parameter estimation accuracies ranging from 0.6 to 0.02 deg for misalignment and 0.05 deg/1000 s to less than 0.001 deg/1000 s for rate biases were achieved using these two configurations.

While the absolute accuracies presented can be improved by an optimal choice of antenna configurations and the use of multiple measurements coincident in time,[6] the present analysis clearly indicates the feasibility of interferometric attitude determination and parameter estimation using the Global Positioning System. In addition, integration of a long baseline interferometer with optical and RF calibration provides the basis for sophisticated figure and attitude control systems on large structures, and arrays currently being investigated for future power and communications platforms.

Acknowledgments

This work was supported by Lockheed Missiles and Space Company under an independent development program. The authors gratefully acknowledge J. G. Charitat and D. Herber for their support and valuable discussions, along with B. Michael and S. Dekany for their artistic contributions.

References

[1] Teichman, M.A., Marek, F.L., Browing, J.J., and Parr, A.K., "The ATS-F Interferometer—A Precision Wide Field-of-View Attitude Sensor," *Communication Satellite Developments: Technology,* edited by W.G. Schmidt and G.E. LaVean, AIAA, New York, 1976, pp. 35-48.

[2] Spinney, V.W., "Applications of the Global Positioning System as an Attitude Reference for Near Earth Users," presented at ION National Aerospace Meeting, April 1976, Navel Air Development Center, Warminster, Pa.

[3] Coffman, V.D., "On-Line Estimation of Gyro Parameters Using Experimentally Developed Gyro Models, and other Applications," Dept. of Aeronautics and Astronautics, Stanford University, Stanford, Calif., SUNDAR No. 467, Dec. 1973.

[4] Coffman, V.D. and DeBra, D.B., "Estimation of Gyro Parameters for Experimentally Developed Gyro Models," AIAA Paper 75-1071, Boston, Mass., Aug. 1975.

[5] Bryson, A.E., and Ho, Y.C., *Applied Optimal Control,* Blaisdell Publishing Co., Waltham, Mass., 1969.

[6] Bogen, A.H., "Geometric Performance of the Global Positioning System," SAMSO-TR-74-169, June 1974.